JOURNAL OF MATERIALS SCIENCE 19 (1984) 3389–3398

Towards equilibrium during tempering a high-speed steel

C. S. WRIGHT*
School of Materials Science, University of Bradford, West Yorkshire, UK
R. S. IRANI†
Division of Materials Applications, National Physical Laboratory, Teddington, UK

The present investigation outlines the sequence of secondary carbide precipitation at various stages of tempering a quenched T42 high-speed steel. Samples from both conventional cast and wrought and the more recently developed powder metallurgy routes have been studied. By using a Holloman and Jaffe construction combined with transmission electron microscopy, it has been possible to follow the influence of various microstructural features and their evolution on mechanical properties. It was established that while the production route had no apparent effect on the observed precipitation reaction, MC type carbides were the primary contribution to the secondary hardening phenomenon. Furthermore, by studying overaged microstructures it has been possible to suggest a probable reason for the degradation of cutting tools during service.

1. Introduction

High-speed steels (HSS) are a commercially important group of ferrous alloys used primarily in the metal cutting and forming industries. They possess high strength, particularly at temperatures experienced during service, combined with good toughness and wear resistance. In the annealed condition the microstructure of HSS consists of a dispersion of alloy carbides primarily of the types M_6C, MC and $M_{23}C_6$, where M denotes the metallic constituents. During commercial austenitizing treatments all the $M_{23}C_6$ carbides, along with some of the M_6C carbides, are taken into solution. On subsequent tempering, in the range 500 to 560° C, a fine dispersion of alloy carbides precipitates in the martensite, producing a precipitation hardened matrix [1]. It is this precipitation hardening that is believed to be largely responsible for the attractive cutting properties of these alloys. Work has shown that the hardening precipitate may be M_2C [2, 3] or MC [4–6], though less is known about carbide precipitation in these steels than for low alloy steels [7].

Although most HSS are still produced by conventional cast and wrought (CW) techniques, an increasing amount is being manufactured by powder metallurgy (PM) processing routes. The PM steels are free of the carbide banding and segregation which characterizes the CW steels.

Recently, preliminary findings on the tempering behaviour of a tungsten-based T42 HSS have been reported by Irani *et al.* [8]. The present paper gives a more detailed description of tempering reactions in this grade of HSS. In order to study the effects that a processing route may have on the tempering behaviour, both CW and PM products were investigated.

2. Experimental procedure

2.1. Materials/heat treatment/metallography

Cast and wrought T42 high-speed steel was obtained in the form of an annealed hot-rolled bar. The starting material for the sintered samples was a water-atomized powder which was annealed, die pressed and vacuum sintered [9]. Following

*Present address: Department of Metallurgy, University of Strathclyde, Glasgow, UK.
†Present address: Manager, Cylinders and Metallurgy, BOC Ltd, Great West House, Great West Road, Brentford, Middlesex, UK.

0022–2461/84 $03.00 + .12

TABLE I Chemical composition of annealed CW and PM T42 used in this investigation

Material	Element (wt%)							
	C	Si	Mn	Cr	Mo	W	V	Co
CW T42	1.31	0.30	0.26	3.89	2.38	8.76	2.71	8.90
PM T42	1.37	0.32	0.20	4.42	3.10	9.81	2.74	9.26

sintering the fully dense samples were annealed. The chemical compositions of both wrought and sintered materials are presented in Table I.

The wrought and sintered steels were cut into specimens with dimensions of 15 mm x 15 mm x 5 mm. These were subsequently pre-heated at 850° C for 0.5 h followed by austenitization at 1175° C. After holding for 2.5 min the samples were quenched into a salt bath at 550° C and then air cooled to room temperature. Samples were subsequently tempered for a variety of times at selected temperatures in the range 450 to 750° C and the microstructures obtained were characterized.

Thin foils suitable for transmission electron microscopy were prepared by first spark machining 0.5 mm thick slices from bulk samples. These were lapped to ~ 0.075 mm. Discs, 3 mm in diameter, were punched from the lapped foils and ion-beam thinned using an Edwards IBT200 machine. The foils were examined using an AEI EM7 high voltage electron microscope fitted with a Link Systems 860 energy-dispersive microanalysis unit.

For the preparation of carbon extraction replicas, samples were ground on silicon carbide papers and polished on cloths impregnated with 6 and 1 μm diamond pastes. Polishing was completed using a slurry of γ-alumina and water. After etching for about 10 sec in 2% nital a thin film of carbon was deposited on the etched surface. This film was released by re-etching in 2% nital. The replicas were supported on copper microscope grids.

For optical microscopy, samples were etched in nital and examined using a Reichert Univar microscope. Hardness tests were conducted with a Vickers machine at a load of 50 kg.

3. Results

3.1. As-quenched microstructure

After quenching into molten salt at 550° C and air cooling the microstructure of the cast and wrought and sintered steels consisted of coarse undissolved primary carbides dispersed in a martensitic matrix (Figs. 1a and b). The matrix for both processing routes was similar in appearance, consisting of internally twinned plate martensite (Fig. 1c) and areas of retained austenite.

Analysis of selected area electron diffraction patterns showed that the undissolved carbides were MC and M_6C. These two phases had characteristic compositions, (Figs. 2a and b) and were similar for the two types of HSS products. Furthermore, it was an easy task to discriminate between these two phases metallographically, in conjunction with thin-film interference microscopy. The M_6C carbides were rich in iron, tungsten and molybdenum with the presence of some chromium and vanadium, whereas the MC phase was primarily vanadium carbide with a low solubility of iron, tungsten and molybdenum. Once the relationship between electron diffraction and composition had been established, it was easier to identify carbides by means of their characteristic spectra rather than by electron diffraction.

3.2. Variation in hardness on tempering

Holloman and Jaffe [10] have shown that during the tempering of steel, time and temperature can be related by a tempering parameter (Q) in the form $Q = T(C + \ln t)$ where T is temperature (° C), t is time (sec) and C is a constant, which for many alloy and tool steels is taken as 20 [11]. The variation in room-temperature hardness on tempering of both CW and PM T42 is shown in Fig. 3. Because a variety of tempering conditions were employed, the hardness data are shown plotted against the Holloman–Jaffe parameter mentioned above. As can be seen, a smooth curve could be fitted to the hardness data, with both steels showing a peak hardness of 1000 HV50, produced by tempering at 525° C for 3 x 1.5 h (Q = 12 933). Both products exhibited similar characteristics on tempering.

4. Discussion

4.1. Microstructural changes during tempering

4.1.1. Tempering at 450° C

Triple tempering for (3 x 1.5 h) at 450° C, equivalent to a tempering parameter, Q = 13 360, pro-

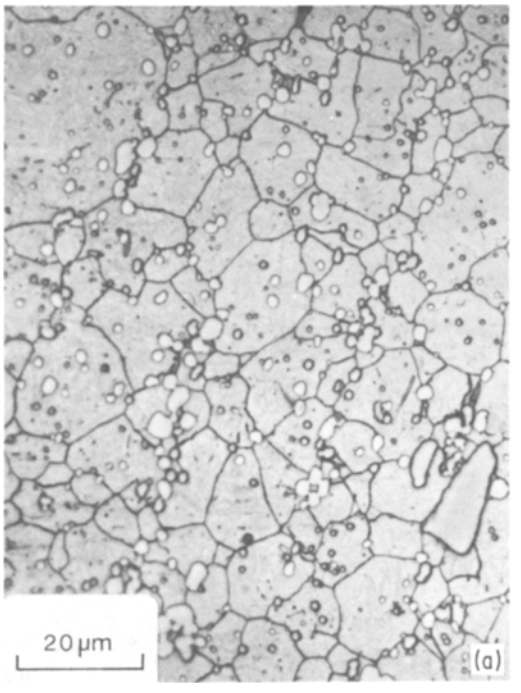

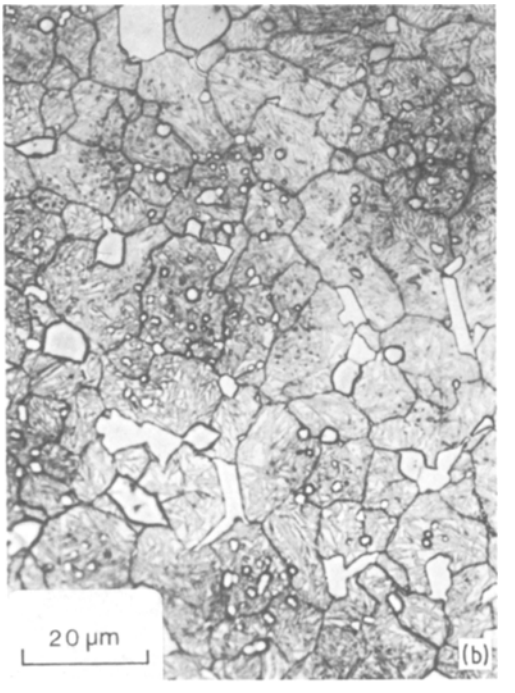

Figure 1 As-quenched optical microstructures of (a) CW and (b) PM high-speed steels, and (c) electron micrograph of internal twinning within martensite.

duced samples which were undertempered (see Fig. 3). TEM examination of both CW and PM steels showed that the retained austenite had transformed to internally twinned martensite. Acicular precipitates, identified by electron diffraction as cementite, were detected in some of the martensite plates (Fig. 4). It would appear that the cementite precipitates had been nucleated at the internal twin boundaries, a mode of precipitation previously observed in tempered ferrous martensites [12, 13]. Apart from a mottling in the matrix (Fig. 5) there was no other evidence to suggest that any other carbides had been precipitated during tempering. The mottled structure was, as shown in Fig. 4, directional in nature, possibly due to precipitation on ⟨1 0 0⟩ matrix planes.

4.1.2. Tempering at 525° C

After tempering to peak hardness the martensitic structure of both steels was similar in appearance to that observed at 450° C, with acicular precipitates of cementite present in a few of the individual martensite plates. Observations would suggest that a smaller amount of cementite was present in structures tempered to peak hardness than in those tempered at 450° C. It was noticeable that a dispersion of fine small carbides,

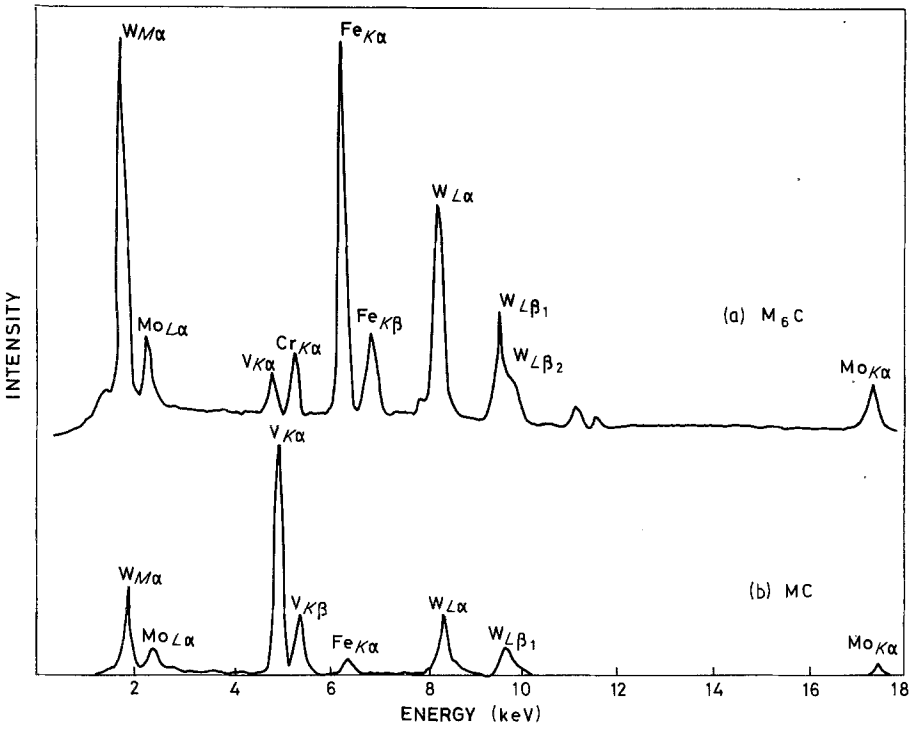

Figure 2 Typical energy dispersive X-ray spectra of M_6C and MC primary carbides.

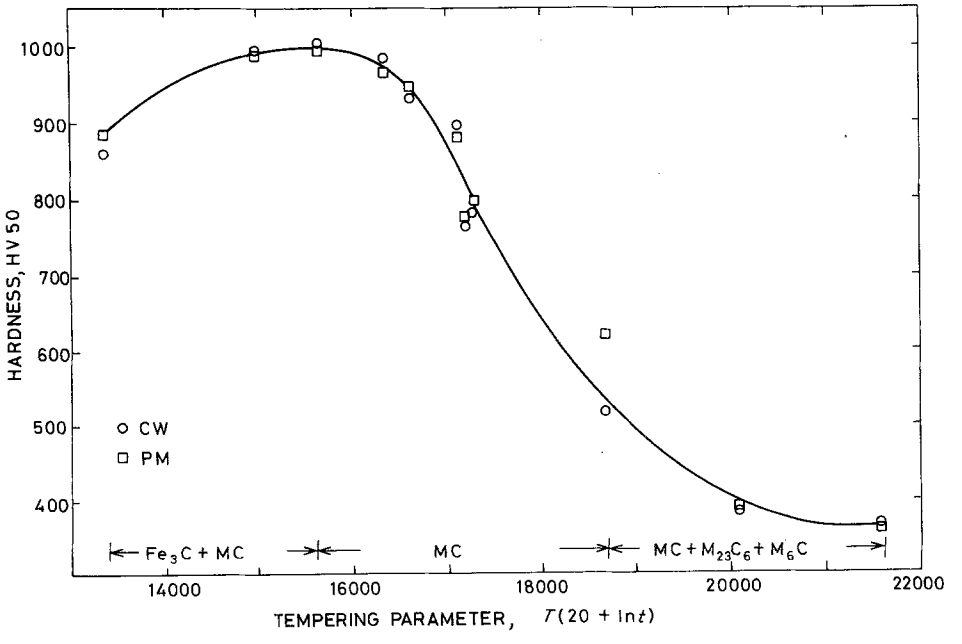

Figure 3 Variation in hardness with tempering conditions for CW and PM T42.

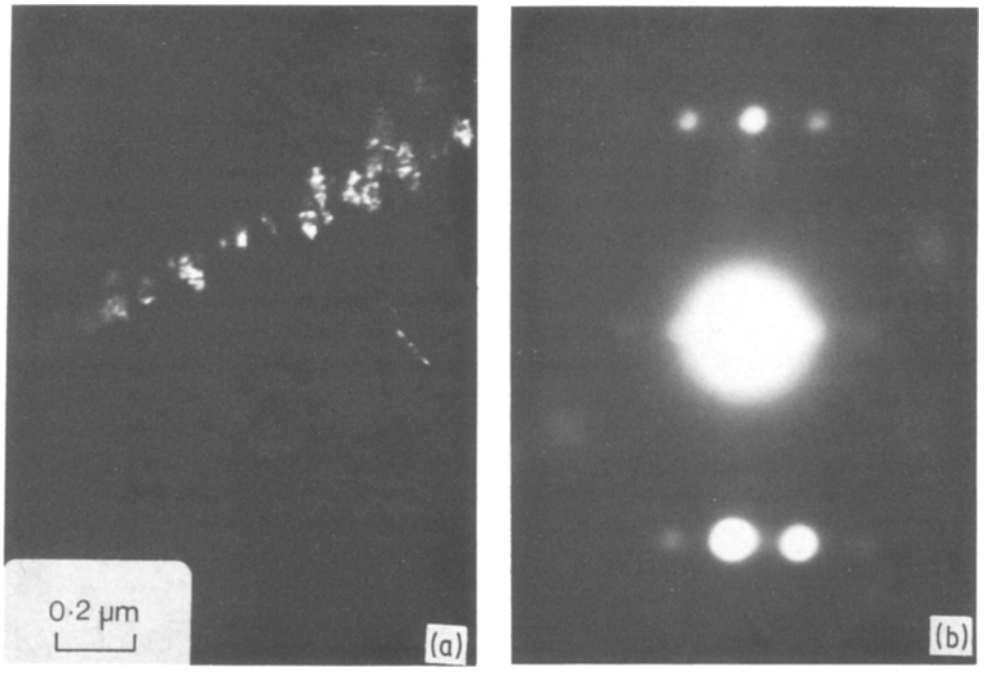

Figure 4 (a) Dark field image of cementite needles precipitated in CW T42 tempered at 450° C for 4.5 h. The image was formed using the cementite reflection in (b). (b) Diffraction pattern of (a) (beam direction = $\langle 1\,2\,0\rangle_{Fe_3C}$).

~ 10 nm long, has been precipitated in the martensite (Fig. 6). Diffraction patterns from these areas occasionally possessed a set of rings. Subsequent analysis of these ring patterns indicated that the fine precipitates were $MC(V_4C_3)$ carbides. In tempered martensite MC carbides are known to precipitate, as platelets, on $\{1\,0\,0\}$ habit planes [14–16] and the orientation relationship between the ferritic matrix and precipitate is described by the Baker–Nutting [17] relationship

$$\{1\,0\,0\}_{MC} \parallel \{1\,0\,0\}_{\alpha}$$
$$\langle 1\,0\,0\rangle_{MC} \parallel \langle 1\,1\,0\rangle_{\alpha}$$

The formation of coherent zones or precipitates on $\{1\,0\,0\}$ habit planes will give rise to diffraction spots which are streaked in $\{1\,0\,0\}$ directions. Such streaking was observed when foils of CW and PM T42 were orientated so that the electron beam was parallel to either $\langle 1\,0\,0\rangle$ or $\langle 1\,1\,0\rangle$ zone axis, e.g. Fig. 7.

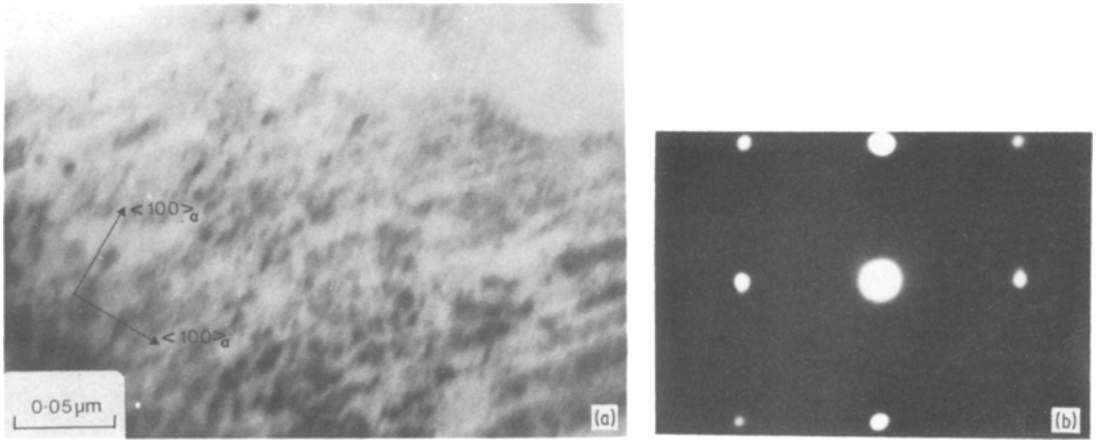

Figure 5 (a) Mottled substructure in CW T42 tempered at 450° C for 4.5 h, and (b) corresponding diffraction pattern (beam direction = $\langle 1\,0\,0\rangle_{\alpha}$).

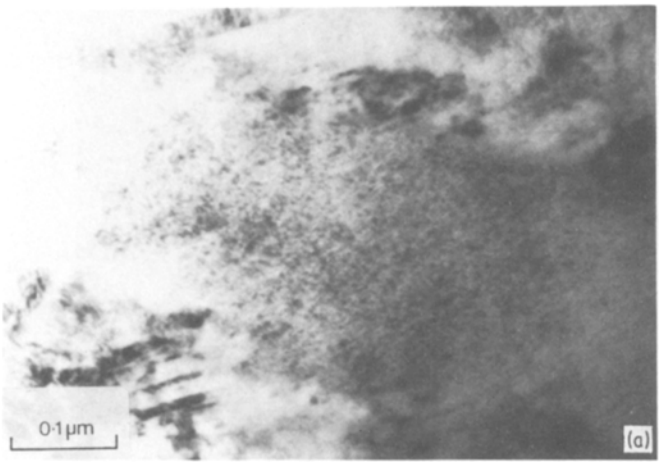

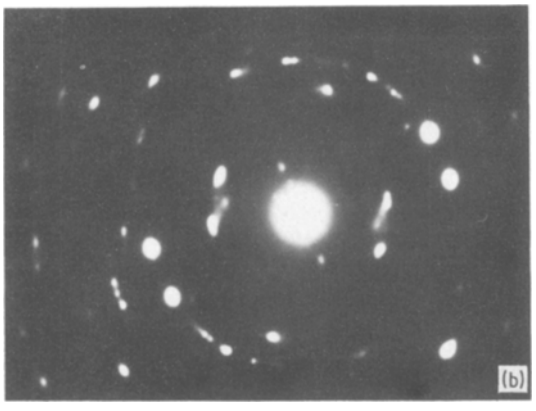

Figure 6 (a) Dispersion of MC carbides precipitated in PM T42 tempered at 525° C for 4.5 h, and (b) corresponding diffraction pattern – note rings.

4.1.3. Tempering at 650° C

After overageing, as a result of tempering at 650° C for 1.5 h ($Q = 18\,590$) the martensite in both steels had begun to decompose. Although the structure was lath-like, very few martensite plates showed any evidence of internal twinning. The MC dispersion had coarsened enabling individual precipitates to be resolved (Fig. 8). In addition, other carbides were detected in the microstructures. These precipitates had formed either in the matrix surrounding MC and M_6C primary carbides (Fig. 9) or at martensite lath boundaries.

4.1.4. Tempering at 750° C

Following tempering at 750° C for 1.5 h ($Q = 214\,500$) the matrix had largely recrystallized to give a structure of equiaxed ferrite grains with coarse tempered carbides at the grain boundaries (Fig. 10a). As with the samples tempered at 650° C these coarse carbides were also detected around undissolved MC and M_6C carbides. In certain regions the matrix retained a lath-like martensite appearance. Coarse carbides had formed at the lath boundaries whereas distinct MC platelets were observed within the laths (Fig. 10b). In a recent paper [8] we suggested that, from analysis of electron diffraction patterns, the coarse tempered carbides observed in overaged T42 were M_6C and $M_{23}C_6$. Microanalysis of these carbides, extracted on carbon replicas, confirmed the electron diffraction results. Typical EDS spectra for the M_6C and $M_{23}C_6$ phases are shown in Figs. 11a and b, respectively. The M_6C carbides were richer in chromium than the primary M_6C carbides (cf. Figs. 2a and 11a). The $M_{23}C_6$ carbides were rich in iron and chromium with solubility for tungsten, molybdenum and vanadium.

Hence by using TEM it has been possible to observe and identify the carbides precipitated at various stages during the tempering of CW and PM T42 HSS. The production route had no effect on the observed carbide precipitation. In both cases secondary hardening was caused by the precipitation of MC carbides, thereby confirming some tentative results of Irani *et al.* [8]. The orientation relationship between matrix and precipitate was not determined but the streaking of matrix diffraction spots in ⟨1 0 0⟩ directions (Fig. 7) due to the nucleation and growth of the MC carbides on {1 0 0} habit planes, is consistent with the Baker–Nutting relationship [17]. In Fig. 7 these MC carbides can clearly be seen lying on {1 0 0} habit planes.

In samples tempered to just below peak hardness it was noted that the matrix was mottled (see Fig. 5). It is believed that this mottling is due to the precipitation of MC carbides on {1 0 0} planes though, due to the lack of corroborative diffraction data, this must be considered tentative.

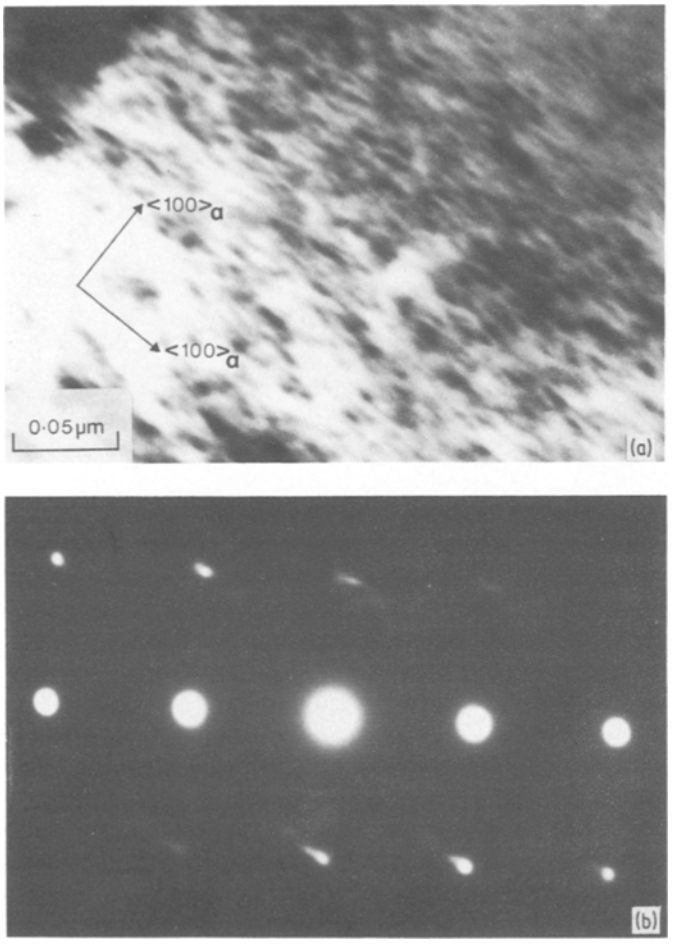

Figure 7 (a) Transmission electron micrographs showing MC carbides precipitated on $\{1\,0\,0\}_\alpha$ planes, and (b) corresponding diffraction pattern (beam direction = $\langle 1\,0\,0\rangle_\alpha$).

At peak hardness, the MC dispersion had developed to the optimum in terms of precipitate size and spacing. The size of the MC platelets at peak hardness (i.e. ~ 7.5 nm across) is comparable to that observed in low alloy vanadium steels [14, 16] and high-speed steels [6].

The TEM observations would suggest that the following precipitation sequence occurs when CW and PM T42 is tempered:

$$Fe_3C \rightarrow MC \rightarrow MC + M_{23}C_6 + M_6C$$

The presence of cementite in under-tempered HSS has been observed by other workers [2, 4]. It is believed that the cementite precipitates, detected in samples of T42 tempered just below or at peak hardness, had formed prior to the MC carbides. At 600° C enthalpies of formation for vanadium carbide and cementite are $-117.5\,kJ\,mol^{-1}$ and $+25.1\,kJ\,mol^{-1}$, respectively [18]. Hence, on a thermodynamic basis, vanadium carbide would be more stable than cementite so would be expected to form in preference to cementite when T42 is tempered in the vicinity of the secondary hardening peak. This consideration neglects the importance that the diffusion rates of the various alloying elements in martensite will have upon carbide formation. At temperatures below 525° C the diffusion rate for carbon in ferrite is much higher than the corresponding rate for vanadium. It is reasonable to assume that the growth of cementite is governed by the diffusion of carbon whilst the growth of the MC precipitates is determined by the diffusion of vanadium. Hence cementite will form initially in preference to MC. Because the amount of cementite is lower in samples tempered to peak hardness than on those tempered below the secondary hardening peak it would appear that cementite is being replaced by the more stable MC precipitates. It is not possible to say whether this replacement occurs by either *in situ* or "separate development" mechanisms, though the latter is more likely since this is the

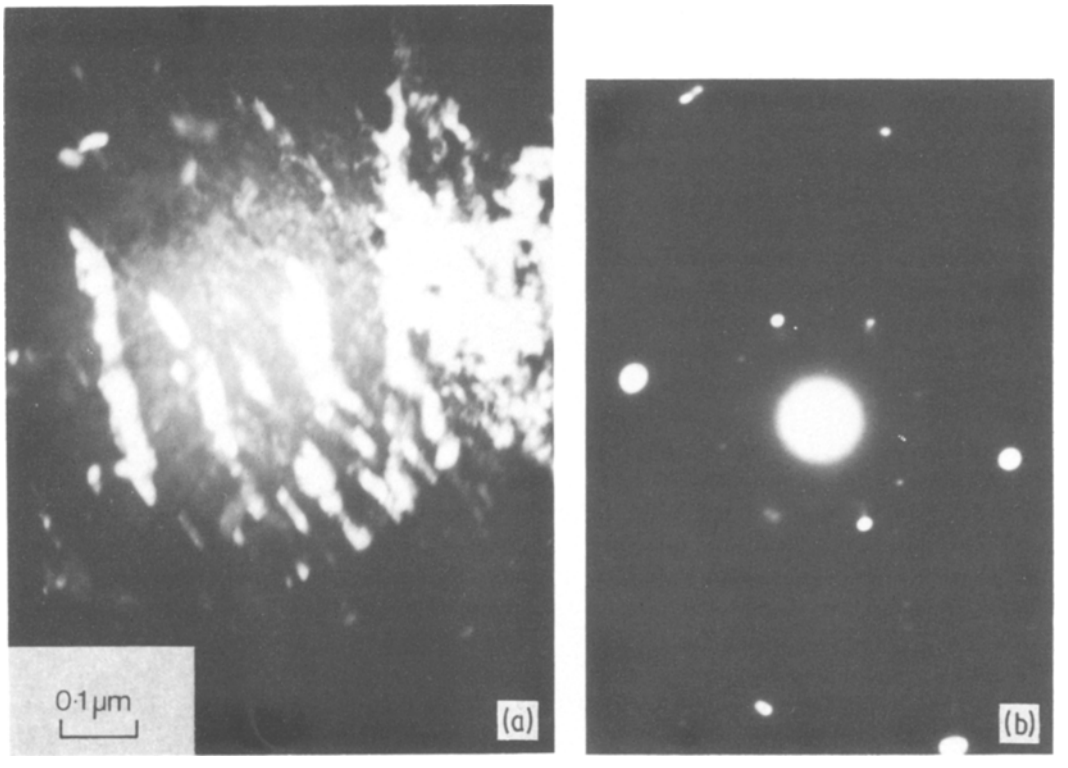

Figure 8 PM T42 overaged at 650° C for 1.5 h. (a) Dark field image of MC precipitates obtained using the MC {1 1 1} reflection. (b) Diffraction pattern of the area shown in (a).

mechanism observed in secondary hardening steels [7].

Initially, overageing in T42 occurs as a result of coarsening of the MC dispersion. Later in the overageing process softening occurs due to the decomposition of the martensite and the precipitation and subsequent coarsening of $M_{23}C_6$ and M_6C carbides. Unlike steels precipitation hardened by a dispersion of M_2C carbides, which redissolve to be replaced by $M_{23}C_6$ carbides during ageing [7], there is no evidence to suggest that the MC dispersion redissolves in overaged T42. Instead, in the overaged structures the $M_{23}C_6$ and M_6C precipitate as well as MC. An interesting feature of the overaged structures was the presence of satellites of secondary $M_{23}C_6$ and M_6C carbides around primary carbides. These satellites have been observed in other HSS [6, 20] as well as T42

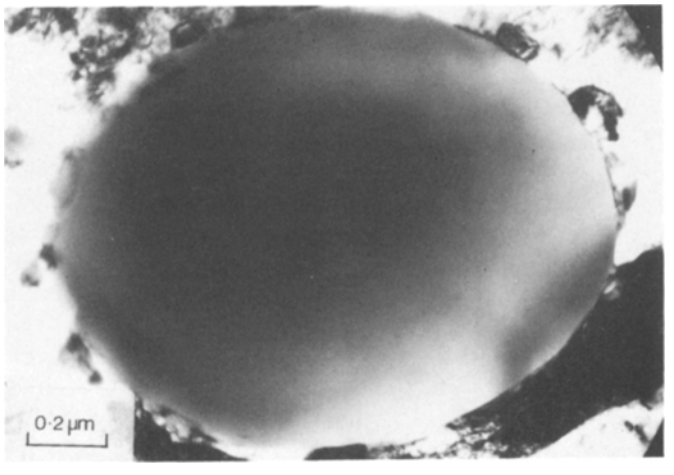

Figure 9 Transmission electron micrographs of CW T42 tempered at 650° C for 1.5 h showing a large MC primary carbide. Note the precipitation of smaller tempered carbides at the primary carbide–matrix interface.

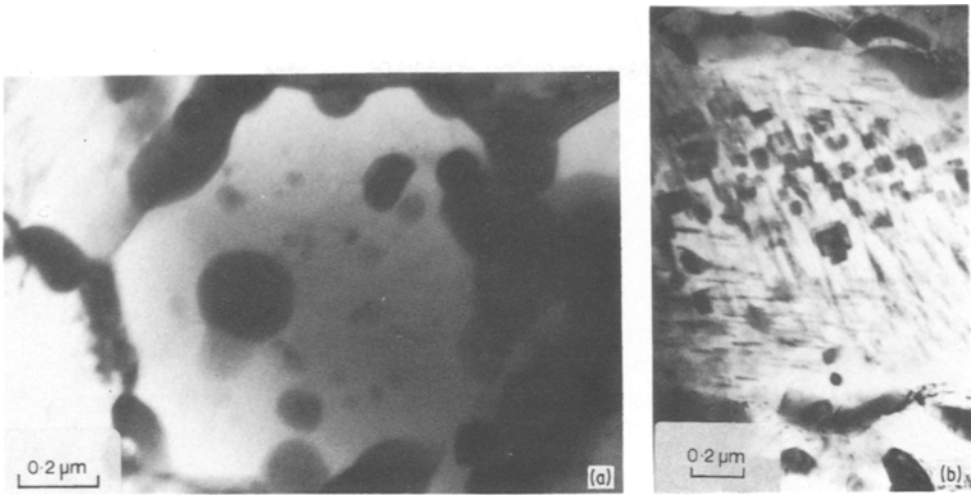

Figure 10 Microstructure of PM T42 tempered at 750° C for 1.5 h. (a) Recrystallized matrix with M_6C and $M_{23}C_6$ carbides precipitated at ferrite grain boundaries. (b) MC carbides precipitated within a former martensite lath. Note $M_{23}C_6$ and M_6C precipitated at the lath boundaries.

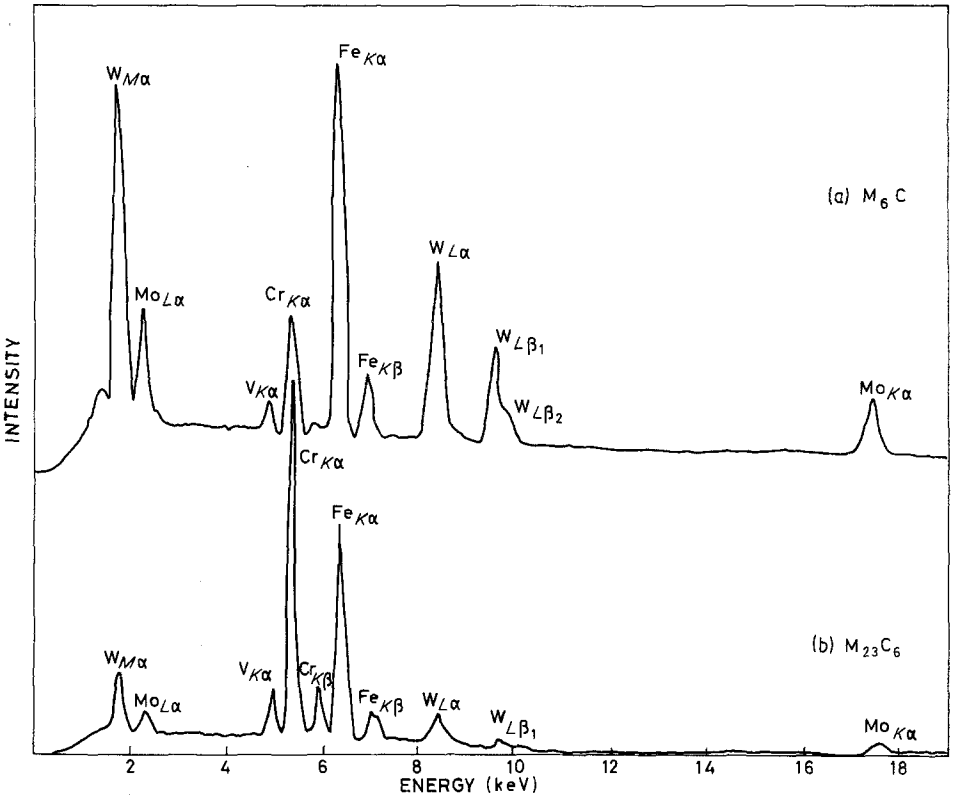

Figure 11 Typical energy dispersive spectra for M_6C and $M_{23}C_6$ carbides precipitated in T42 high-speed steel tempered at 750° C for 1.5 h.

[8]. It is believed that solute-rich zones, produced during austenitization, 1 to 2 μm in extent surround the undissolved primary carbides. The resulting concentration gradient provides the necessary driving force for the growth of the satellite carbides [8].

During service high-speed steel cutting tools may experience similar temperatures to those used during tempering [19]. It is interesting to speculate that there may be a possibility that the microstructural changes observed during tempering may occur during a cutting tool's life. If so, it may account to some extent for the degradation of cutting tools during service. In order to confirm this view it will be necessary to conduct a detailed electron microscopical study of used tools.

References

1. T. D. ATTERBURY, *Metall. Met. Form.* (1971) 210.
2. R. TEKUN and M. H. RICHMAN, *Metallography* **3** (1970) 327.
3. L. COLOMBIER and R. LEVEQUE, *Mém. Sci. Rev. Mét.* **65** (1968) 229.
4. T. MUKHERJEE, "Materials for Metal Cutting", ISI Special Issue No. 127 (1970) pp. 80–96.
5. E. HORN, *DEW Technische Berichte* **13** (1974) 171.
6. L. E. SVENSSON *et al.*, "Quantitative Microscopy with High Spatial Resolution" (Metals Society, London, 1982) p. 256.
7. R. W. K. HONEYCOMBE, Strength and Structure of Alloy Steels (Climax Molybdenum Co. 1974).
8. R. S. IRANI, C. S. WRIGHT and A. S. WRONSKI, *J. Mater. Sci. Lett.* **1** (1982) 918.
9. E. A. DICKINSON and P. I. WALKER, Metal Powder Report (February, 1980).
10. J. H. HOLLOMAN and L. D. JAFFE, *Trans. AIME* **162** (1945) 223.
11. P. PAYSON, "Metallurgy of Tool Steels" (Wiley, 1962) p. 139.
12. P. M. KELLY and J. NUTTING, *Proc. Roy. Soc.* **259A** (1961) 45.
13. G. R. SPEICH and W. C. LESLIE, *Met. Trans.* **3** (1972) 1043.
14. E. TEKIN and P. M. KELLY, *J. Iron Steel Inst.* **203** (1965) 715.
15. D. RAYNOR, J. A. WHITEMAN and R. W. K. HONEYCOMBE, *ibid.* **204** (1966) 349.
16. E. SMITH, *Acta Metall.* **14** (1966) 583.
17. R. G. BAKER and J. NUTTING, Precipitation Processes in Steels, ISI Special Issue No. 64 (1964).
18. C. E. WICKS and R. E. BLOCK, "Thermodynamic Properties of 65 Elements – Their Oxides, Halides, Carbides and Nitrides" (US Government Printing Office, Washington, 1963) p. 61.
19. P. K. WRIGHT and E. D. TRENT, *J. Iron Steel. Inst.* **211** (1978) 364.
20. R. S. IRANI, to be published.

Received 15 December 1983
and accepted 16 January 1984